Sensitivities of Earth's core and mantle compositions to accretion and differentiation processes

Rebecca A. Fischer[1,2,3,*], Andrew J. Campbell[1], and Fred J. Ciesla[1]

[1]University of Chicago, Department of the Geophysical Sciences, 5734 S Ellis Ave, Chicago, IL 60637, USA

[2]National Museum of Natural History, Smithsonian Institution, PO Box 37012, MRC 119, Washington, DC 20013-7012

[3]University of California Santa Cruz, Department of Earth and Planetary Sciences, 1156 High St, Santa Cruz, CA 95064

*Corresponding author. Phone: (202) 633-1801. Email: fischerr@si.edu

Accepted for publication in Earth and Planetary Science Letters

15 October 2016

Abstract

The Earth and other terrestrial planets formed through the accretion of smaller bodies, with their core and mantle compositions primarily set by metal–silicate interactions during accretion. The conditions of these interactions are poorly understood, but could provide insight into the mechanisms of planetary core formation and the composition of Earth's core. Here we present modeling of Earth's core formation, combining results of 100 *N*-body accretion simulations with high pressure-temperature metal–silicate partitioning experiments. We explored how various aspects of accretion and core formation influence the resulting core and mantle

chemistry: depth of equilibration, amounts of metal and silicate that equilibrate, initial distribution of oxidation states in the disk, temperature distribution in the planet, and target:impactor ratio of equilibrating silicate. Virtually all sets of model parameters that are able to reproduce the Earth's mantle composition result in at least several weight percent of both silicon and oxygen in the core, with more silicon than oxygen. This implies that the core's light element budget may be dominated by these elements, and is consistent with ≤1–2 wt% of other light elements. Reproducing geochemical and geophysical constraints requires that Earth formed from reduced materials that equilibrated at temperatures near or slightly above the mantle liquidus during accretion. The results indicate a strong tradeoff between the compositional effects of the depth of equilibration and the amounts of metal and silicate that equilibrate, so these aspects should be targeted in future studies aiming to better understand core formation conditions. Over the range of allowed parameter space, core and mantle compositions are most sensitive to these factors as well as stochastic variations in what the planet accreted as a function of time, so tighter constraints on these parameters will lead to an improved understanding of Earth's core composition.

Keywords

Core formation, core composition, metal–silicate partitioning, accretion, light elements, trace elements

Highlights

- Combined accretion simulations and partitioning experiments to model core formation
- Si and O most likely dominate light element budget of Earth's core

- Earth formed from reduced materials at temperatures near or slightly above liquidus
- Tradeoff between equilibration depth and amount of metal and silicate equilibrating
- Core and mantle compositions most sensitive to these factors plus accretion history

1. Introduction

The metal–silicate differentiation of the Earth, which occurred simultaneously with accretion, was the primary determinant of the Earth's modern-day core and mantle compositions. During the planet's formation, accretion of material occurred through energetic impacts, causing large-scale melting on the Earth and generating a partial or global magma ocean. Metal from impactors equilibrated with molten silicate at high pressures (P) and temperatures (T) before being segregated into the growing core. These high P-T reactions set the compositions of the core and mantle, which today provide geochemical and geophysical signatures of the core formation process.

One signature of this process is Earth's core density, which is ~10% lower than that of iron under the same P-T conditions, due to the presence of lighter elements such as Si, O, S, C, and/or H (e.g., Birch, 1952; Poirier, 1994; McDonough, 2003) that primarily entered the core during its formation. Density and sound velocity measurements of Fe alloys can be compared to the core's properties to put upper bounds on its light element abundances, such as ~8 wt% O or ~11 wt% Si (e.g., Fischer et al., 2011, 2014; Sata et al., 2010; Zhang et al., 2014; but also cf. Badro et al., 2015, and references therein), but the relative proportions of light elements in the core remains an open question. The core's light element composition relates to the devolatilization and redox history of the planet's interior, as well as Earth's bulk elemental and isotopic composition. These elements influence the core's thermal structure, crystal structures

and anisotropy, thermal conductivity, and convection and magnetic field generation (e.g., Fischer et al., 2013; McDonough, 2003; Nimmo, 2007).

To constrain the relative proportions of light elements in the Earth's core and gain insight into the core formation process on terrestrial planets, here we combine *N*-body accretion simulations with experimental metal–silicate partitioning data to model core formation. Previous studies have combined *N*-body simulations with condensation models to calculate bulk planetary compositions (Bond et al., 2010; Elser et al., 2012) without consideration of core formation, or modeled core formation using a prescribed growth scenario to describe Earth's accretion (e.g., Badro et al., 2015; Rubie et al., 2011), which is less realistic than using accretion simulations due to the highly stochastic nature of accretion and which may not be representative of Earth's formation. Many studies imposed a constant or variable oxygen fugacity (fO_2) instead of allowing it to evolve as a consequence of partitioning (e.g., Badro et al., 2015; Siebert et al., 2012, 2013; Wade and Wood, 2005; Wood et al., 2014). Rubie et al. (2015) were pioneering in their fusion of accretion simulations and core formation modeling, utilizing six simulations run under the Grand Tack paradigm (Walsh et al., 2011) and allowing planetary oxygen fugacity to evolve self-consistently. They predicted a core composition of 8–9 wt% Si and 2–4 wt% O, and varied the initial compositions of planetary building blocks to best reproduce the composition of the Earth's mantle.

Here we take a different approach, using forward modeling to explore how different aspects of Earth's accretion and core formation influence the resulting core and mantle compositions. We take advantage of recent advances in metal–silicate partitioning experiments to higher pressures and temperatures (e.g., Bouhifd and Jephcoat, 2011; Fischer et al., 2015; Siebert et al., 2012, 2013) and in *N*-body simulations, utilizing a large number of simulations

93 (Fischer and Ciesla, 2014) to statistically analyze the results. Our goal is not to find one set of
94 model parameters that best reproduces the Earth, due to the many inherent uncertainties
95 involved, but rather to explore these uncertainties by assessing the effects of accretion and
96 differentiation on the resulting planetary composition. In this way, we can evaluate which of
97 these processes exert the most influence on planetary chemistry and are the least well-
98 constrained, so that future experimental and numerical studies may be better targeted.
99 We begin by describing the numerical methodology (Section 2), then the resulting core
100 and mantle compositions (Section 3) and the effects of different aspects of accretion and core
101 formation (Section 4). These results are discussed in terms of tradeoffs, constraints, and
102 sensitivities to various processes; limitations of the modeling; and future directions (Section 5),
103 followed by concluding remarks (Section 6).
104
105 **2. Methods**
106 From the 100 *N*-body simulations of Fischer and Ciesla (2014), 73 Earth analogues were
107 identified, defined as planets with final semimajor axes of 0.75–1.25 AU and masses within a
108 factor of 1.5 of an Earth mass ($M_{\oplus}$). These high-resolution simulations were run with Jupiter and
109 Saturn on either their modern-day orbits (Eccentric Jupiter and Saturn, EJS) or more circular
110 orbits, as predicted by the Nice Model (e.g., Tsiganis et al., 2005) (Circular Jupiter and Saturn,
111 CJS). The initial conditions were similar to those of previous studies (e.g., Raymond et al.,
112 2009). For more details on these simulations, see the Supplemental Text or Fischer and Ciesla
113 (2014). Fischer and Ciesla (2014) reported a lack of correlations between most Solar System
114 observables, indicating that any simulations that form a realistic Earth analogue can provide a
115 plausible accretion history for the Earth, even if they do not match every other aspect of the Solar

System. Figure 1 illustrates the types of information about Earth's accretion history that can be gleaned from these simulations, showing the Earth analogue's mass (bottom panel) and the initial semimajor axis of everything it accretes (top panel) as a function of time in a few simulations chosen as illustrative examples.

Each body in every simulation was assigned an initial composition based on its initial semimajor orbital axis. These compositions were calculated by equilibrating a CI chondrite enriched in refractory elements at 0.1 GPa and 2000 K, with the oxygen content varied to reach a specified fO_2. Starting compositions are presented in Table S1. With each impact that the Earth analogue experienced, its pressure distribution was recalculated. The incoming metal and silicate were equilibrated by first calculating their major element compositions, then their trace element compositions, then the resulting metal and silicate were added to the core and mantle. This process was repeated for each body that the Earth analogue accreted.

Equilibration occurred at a fixed fraction of the target's core–mantle boundary (CMB) pressure at the time of impact and the mantle liquidus temperature at that pressure (Andrault et al., 2011). The methodology for the chemical model was inspired by that of Rubie et al. (2011), in which oxygen fugacity evolved self-consistently as the Earth grew as a consequence of metal–silicate partitioning, as opposed to being imposed. Partitioning was based on experimentally-determined metal–silicate partition coefficients (Fischer et al., 2015, and references therein), including new fits to data from $P < 5$ GPa (Supplemental Text; Table S2). Equilibrated metal and silicate compositions were calculated using mass balance equations and equations of the form:

$$log_{10}\left(K_D^i\right) = a_i + \frac{b_i}{T} + \frac{c_i P}{T} \quad (1)$$

for each element i, where T is in Kelvin, P is in GPa, and a_i, b_i, and c_i are fitting parameters from Fischer et al. (2015) (Table S2). Effects of metallic melt composition were also included for

some elements (Supplemental Text). The exchange coefficient K_D is defined for a metal M with valence n as:

$$K_D = \frac{D_M}{{D_{Fe}}^{n/2}} = \frac{X_M^{met}/X_{MO_{n/2}}^{sil}}{\left(X_{Fe}^{met}/X_{FeO}^{sil}\right)^{n/2}} \quad (2)$$

where D is a partition coefficient, defined in terms of mole fractions (e.g., X_M^{met} is the mole fraction of M in the metallic melt). For oxygen, the exchange coefficient is $K_D = \frac{X_{Fe}^{met} X_O^{met}}{X_{FeO}^{sil}}$. Ni, Co, Ta, Nb, V, Cr, Si, O, and Fe were exchanged between metal and silicate (for more details, see the Supplemental Text).

For ease of discussion only, we define a set of reference parameters for the core formation model that adequately reproduces the NiO, CoO, and FeO contents of the mantle; core mass fraction; and light element abundances in the core (Table 1). All of the incoming metal equilibrated with all of the impactor's silicate, and none of the target's silicate, at 55% of the target's evolving CMB pressure. The initial oxidation states of the accreted material were described by a step function from IW–3.5 to IW–1.5 (corresponding to silicate FeO contents of 2.2 wt% and 20.4 wt%, respectively; Table S1) at 2 AU. These values represent a plausible range in fO_2 of the majority of Earth's building blocks, with the change in oxidation state correlating with the abrupt change in water contents of asteroids in the main belt (Abe et al., 2000). Similar step function transitions have been used in accretion studies to track water delivery (e.g., Raymond et al., 2009).

There are many aspects of accretion and core formation that are poorly constrained. Here we focus primarily on varying one parameter at a time, to explore its effects on the resulting planetary chemistry. The ranges of each parameter that we tested are listed in Table 1. For example, when assigning initial compositions, uniform distributions of oxygen fugacities of IW–

3.5 or IW–1.5 were used, as well as step functions from IW–3.5 to IW–1.5 with increasing heliocentric distance, with the step at 1.5, 2, or 2.5 AU. Equilibration temperatures were primarily described by the mantle liquidus of Andrault et al. (2011), though temperature distributions shifted by up to –300 K (approximately halfway between the solidus and liquidus) or +600 K (near the liquidus of Fiquet et al. (2010) or superliquidus relative to that of Andrault et al. (2011)) were also tested. A portion of the impactor's silicate always equilibrated, but varying amounts of the target's silicate were sometimes added, from one to ten times the mass of the impactor's silicate (if this exceeded the mass of the target's mantle, the entire mantle was used), representing different extents of equilibration with the target's silicate. In other model runs, the mass of equilibrating silicate was fixed at twice that of the impactor's silicate, while the target:impactor ratio of the equilibrating silicate was varied from 1:1 to 16:1, representing different extents of impactor silicate dispersal upon impact. In cases where the chosen target:impactor ratio exceeded the actual target:impactor silicate ratio, the maximum ratio was used (all of the target's silicate) and the equilibrating silicate mass was kept constant, resulting in a lower target:impactor ratio for some impacts.

3. Results on core and mantle compositions

3.1. The light element composition of Earth's core

Silicon and oxygen contents of the Earth's core increase nearly monotonically during accretion, as shown in Figure 2 (top panel) for the same example simulations as in Figure 1 and the reference parameters used in the core formation model. The effects of fO_2 can be analyzed by comparing results using the reference parameters with those run with all material initially equilibrated at IW–3.5 (the "reduced case") or IW–1.5 (the "oxidized case"), with all other

model parameters fixed at their reference values. Considering the aggregate of all 73 Earth analogues formed in the *N*-body simulations, the reduced case results in more silicon than oxygen in Earth's core, and the oxidized case results in more oxygen than silicon in the core (Figure 3a). The reference set of parameters (including a step function from reduced to oxidized at 2 AU) results in an intermediate composition, but one that more closely resembles the reduced case (Figure 3a). This phenomenon can be understood by considering the evolution of bulk planetary oxygen fugacity, calculated in log units relative to the IW buffer as

$$\Delta\mathrm{IW} = 2\log\left(\frac{X_{FeO}}{X_{Fe}}\right) \quad (3)$$

where X_{FeO} is the mole fraction of FeO in the mantle, X_{Fe} is the mole fraction of Fe in the core, and the approximation of ideal mixing is made. Reduced starting compositions exhibit a larger increase in oxidation state (+1.03 ± 0.16 log units) than more oxidized starting compositions (+0.03 ± 0.05 log units) on average across all Earth analogues (Figure S2). The reference parameter set produces an even larger change in ΔIW (+1.20 ± 0.15 log units) due to the possibility of the Earth accreting oxidized material from the outer disk in the later stages of accretion. The resemblance between the reduced case and reference parameter set is due to the provenance of the Earth analogue: on average, 81% of the mass of the Earth analogue originated inside of 2 AU in CJS cases, and 90% in EJS cases, though there was significant variability between runs (Fischer and Ciesla, 2014). The EJS and CJS simulations have very similar results in the reduced and oxidized cases, but the CJS runs exhibit a slightly higher increase in oxidation state when the reference parameters are used in the core formation model (Figure S2), due to this larger amount of material accreted from outside of 2 AU.

The changes in oxidation state as a function of accretion history can be understood as silicon partitioning more strongly into metal as pressure and temperature increase (e.g., Fischer

et al., 2015; Siebert et al., 2012). As silicon is reduced from 4+ to 0 valence, there must be an exchange of electrons (or equivalently, oxygen) with another species. Iron is the most abundant multivalent element in the Earth, so this exchange is accommodated primarily by the oxidation of iron metal:

$$\mathrm{SiO_2}^{silicate} + 2\mathrm{Fe}^{metal} \leftrightarrow \mathrm{Si}^{metal} + 2\mathrm{FeO}^{silicate} \quad (4)$$

(e.g., Ringwood, 1959). With increasing pressures and temperatures relevant to a growing planet's interior, the reaction described by Eq. 4 is driven toward the right, driving up the bulk planetary oxidation state relative to the IW buffer (Eq. 3). Even in the oxidized case, some silicon partitions into the core as a result of extreme temperatures in the late stages of accretion. Therefore, when oxygen fugacity is calculated self-consistently (as opposed to being imposed), the bulk oxidation state of the planet usually remains constant or increases even in the oxidized case.

All three cases shown in Figure 3a result in a few weight percent, on average, of both silicon and oxygen in the core. This result is not necessarily expected based on experiments at moderate pressures, which suggest that silicon and oxygen are mutually incompatible in the core due to the different oxygen fugacities required to dissolve them into metal (e.g., Malavergne et al., 2004), though recent higher *P-T* experiments report their simultaneous partitioning into metal (e.g., Fischer et al., 2015; Siebert et al., 2012). For all combinations of model parameters explored here that reproduce the mantle's composition, there is more Si than O in the core. The Si/O ratio averaged over all Earth analogues formed in the *N*-body simulations for a given set of core formation model parameters varies from 1.2–7.0 (Table S3).

The light element composition of a planet's core depends on both the planet's size and accretion history. There is a strong correlation between a planetary core's Si/O ratio and the

oxidation state of its accreted material (Figure 3a). If there were independent constraints on the Si/O ratio of the Earth's core (from equation of state, sound velocity, or phase diagram measurements, for example), then one could further constrain the oxidation states of Earth's building blocks. When considering the results from all Earth analogues for a given set of core formation conditions, final core silicon and oxygen contents are correlated both with each other and with final planetary mass (Figure 4). This result indicates that the size of a planet (a proxy for the pressures and temperatures of equilibration), as well as its accretion history, is an important control on its core composition. Accretion history causes additional spread when using the reference parameters in the core formation model due to the random accretion of oxidized material from the outer Solar System, and influences all cases due to variations in *P*-*T* evolution with variable sizes of accreted bodies (e.g., Figure 1). Consideration of more complex effects, like size dependence of the depth or degree of metal–silicate equilibration, should amplify this outcome. The 73 Earth analogues have an average mass of $1.0 \pm 0.2\ M_{\oplus}$, so it is expected that the average compositions are those most valid for the Earth.

The runs shown in Figures 1–2 were chosen as examples because they all produce an Earth analogue with a final mass of ~$0.96\ M_{\oplus}$, so that variations in final composition (and its temporal evolution) are due entirely to stochastic variations in accretion history. The masses and oxidation states of accreted bodies can significantly alter a planet's final composition, even without any variations in the style of core formation, so it is helpful to consider a large number of accretion simulations to better understand the Earth's compositional evolution. All other results discussed here represent an aggregation of all 73 Earth analogues that formed in the *N*-body simulations.

252 Comparisons between mineral physics experiments and geophysical observations of
253 Earth's core density and seismic velocities imply upper bounds on the core's O and Si
254 abundances of ~8 wt% and ~11 wt%, respectively (e.g., Fischer et al., 2011, 2014; Sata et al.,
255 2010; Zhang et al., 2014). The model parameters used here produce a core whose Si+O content
256 is approximately compatible with geophysical observations of the core's density regardless of
257 initial oxidation states (Figure 3a). The density can be matched more precisely by considering
258 the presence of ≤1–2 wt% S and/or C in the core, which are often considered to be the
259 geochemical limits on their core abundances based on their volatilities (e.g., McDonough, 2003)
260 and mineral physics constraints for C (Nakajima et al., 2015; Wood et al., 2013). This study
261 supports these values as upper bounds on the core abundances of S and C while also suggesting
262 non-zero abundances; however, this conclusion will need to be reevaluated when future
263 experimental studies more adequately address the thermodynamic interactions of S and C with Si
264 and O in metallic melts at extreme conditions.
265
266 *3.2. The major and trace element composition of the mantle*
267 Table 2 lists the average mantle and core compositions produced by the reference
268 parameter set. It matches Earth's core mass fraction and observed mantle composition
269 (McDonough and Sun, 1995) within ~2σ for most elements. The modeled compositions in the
270 reduced case are somewhat similar to those from the reference parameters, while those in the
271 oxidized case do not match the Earth's mantle within 2σ for most elements, especially in terms
272 of the mantle FeO content and core mass fraction (Table 2).
273 Using the reference set of core formation parameters, the modeling predicts slightly high
274 values for V_2O_3 and CrO compared to Earth's mantle (Table 2). At least for chromium, this

might reflect volatile loss from the bulk Earth composition, which was not included in the starting compositions. Since V and Cr may be more compatible in lower mantle phases, the observed (upper) mantle composition may underestimate their true abundances in the silicate Earth (Righter, 2015). Experimental metal–silicate partitioning studies of V and Cr at modest pressures show that they both become more siderophile in the presence of carbon and sulfur (e.g., Chabot and Agee, 2003; Mann et al., 2009; Wood et al., 2014). If this interaction remains valid to higher pressures, this result (Table 2) may be suggestive of a small amount of C and/or S in the core. Additionally, the partitioning behaviors of V and Cr exhibit a complex dependence on metal composition that may indicate a valence change, so it is possible that parameterizations of experimental data do not accurately describe their partitioning over all modeling conditions (Fischer et al., 2015). The modeled composition using the reference parameters adequately matches Earth's mantle Nb and Ta abundances, though this finding is preliminary since the partitioning behaviors of these elements have only been measured below 25 GPa (e.g., Mann et al., 2009).

Nickel and cobalt are useful trace elements for considering the conditions of core formation, because their abundances in the Earth are well measured, they are refractory, and they are moderately siderophile, such that their depletions in the mantle are entirely due to core formation. Their partitioning behaviors have been characterized by many previous studies, including in S- and C-free systems relevant to this modeling (Fischer et al., 2015, and references therein). Therefore, this model's ability to reproduce the mantle's Ni and Co abundances is an important test. There is considerable variability among our 73 Earth analogues in their calculated NiO and CoO compositions due to accretionary processes (e.g., Figure 2, bottom panel), but on average they match the Earth well (McDonough and Sun, 1995) (Figure 3b). The same set of

298 reference parameters that reproduce the Earth's core light element composition in terms of its
299 density also reproduce the NiO and CoO contents of the mantle, implying that these model
300 conditions are plausible.
301
302 **4. Effects of different aspects of accretion and core formation**
303 The style of accretion (CJS vs. EJS) has only a minor effect on planetary chemistry when
304 using the reference set of model parameters, due to the accretion of more material from the outer
305 disk in the CJS case (Section 3.1). Table S4 is analogous to Table 2, but shows separate average
306 compositions for the EJS and CJS cases. For example, using the reference model parameters, the
307 EJS and CJS runs produce an average of 2410 and 2600 ppm NiO in the mantle and 5.8 and 5.1
308 wt% Si in the core, respectively. However, variations of similar magnitude can be seen in the
309 reduced and oxidized cases, due to variations in the mass evolution of the Earth analogue.
310 Sensitivities to different aspects of core formation can be assessed by modeling
311 differentiation using the reference parameter set but varying one parameter at a time, and
312 analyzing the aggregate results of all Earth analogues (Figure 5). The resulting core and mantle
313 compositions are extremely sensitive to the depth (pressure and temperature) of metal–silicate
314 equilibration, as shown in Figure 5a and b for core Si content and mantle NiO content (Figure S3
315 is analogous, but for a lower degree of metal–silicate equilibration). Increasing the depth from
316 55% to 60% of the CMB pressure results in a significantly worse match to the Earth on average;
317 for example, it increases mean mantle NiO from 2510 ppm to 2950 ppm and CoO from 133 ppm
318 to 148 ppm (Table S3). Other elements exhibit different behaviors, depending on how their
319 partition coefficients vary with P and T (Figure S4).

320 The initial distributions of compositions and oxidation states in the Solar System are not
321 well known, nor are those of the materials that accreted to form the Earth (e.g., Burbine and
322 O'Brien, 2004; Righter et al., 2006). Though the bulk core light element content (Si+O) does not
323 vary significantly, the Si/O ratio of a planet's core (Figure 3a) and trace element contents of the
324 mantle (Table 2; Figure 5c and d) are sensitive functions of the oxidation states of accreted
325 material. To a limited extent, these compositional aspects can be made to match those of the
326 Earth by simultaneously varying other modeling parameters, such as the depth of equilibration
327 (Section 5.1). However, in the oxidized case, the mantle FeO content and core mass fraction are
328 distinctly different from those of the Earth, and equilibration at shallower depths can not
329 compensate for this large discrepancy. This result differs from some previous studies (Badro et
330 al., 2015; Siebert et al., 2013) due to our self-consistent calculation of oxygen fugacity, discussed
331 above.
332 Planetary composition is sensitive to the fraction of incoming metal that equilibrates
333 (Figure 5e and f). Reducing this fraction significantly lowers the NiO and CoO contents of the
334 mantle and the Si and O contents of the core. For a lower degree of equilibration, the resulting
335 planet partly retains a signature of low pressure core formation from its building blocks, and Ni
336 and Co are more siderophile at lower pressures (e.g., Fischer et al., 2015, and references therein).
337 In addition to shifting the distributions of mantle NiO and CoO contents to lower values,
338 reducing the degree of equilibration also sharpens the distributions. The unequilibrated portion of
339 the impactor's core retains its initial composition, reducing spread in the results due to
340 differences in planetary mass.
341 Varying the target:impactor ratio of the equilibrating silicate for a constant silicate mass
342 has very little effect on the resulting planetary chemistry (Figure 5g and h). Varying the mass of

343 equilibrating silicate by equilibrating with variable amounts of the target silicate does have an
344 effect, but only up to ~3 times the mass of the impactor's silicate (Figure 5i and j). The mass and
345 composition of equilibrating silicate affect the final composition of the mantle more than that of
346 the core. When a larger mass of target silicate equilibrates, its trace element composition is
347 overprinted by equilibration at higher pressures and temperatures in later impacts, resulting in a
348 higher *P-T* signature. This partly explains differences in results obtained in previous models of
349 this kind. Models in which the incoming metal is assumed to equilibrate with the whole mantle
350 (e.g., Wade and Wood, 2005) obtain shallower equilibration depths than models in which the
351 impactor metal exchanges with a smaller fraction of silicate (e.g., Rubie et al., 2011, 2015;
352 Fischer et al., 2015).
353 Variations in equilibration temperature are included in variations with depth, but it is also
354 possible that temperature may vary independently, for example if superliquidus equilibration
355 occurs. There is also disagreement in the literature regarding the liquidus of mantle materials,
356 with the liquidus curve of Fiquet et al. (2010) falling ~500 K higher than that of Andrault et al.
357 (2011) used here. Temperature can be an important factor controlling composition (Figure 5k
358 and l), for example by increasing the siderophility of Si and O (Figure S5), but elements have
359 different sensitivities depending on the temperature dependence of their partition coefficients
360 (Section 5.3; Figure S6).
361
362 **5. Discussion**
363 *5.1. Tradeoffs between different processes*
364 Tradeoffs between the properties discussed in Section 4 can be visualized by considering
365 how the resulting core Si content and mantle NiO content averaged over all 73 Earth analogues

366 change when only one core formation model parameter at a time is varied, with all other
367 parameters held at their reference values (Figure 6). Many of these factors fall along a common
368 axis in their effects on core and mantle compositions: the fraction of metal that equilibrates, mass
369 of equilibrating silicate, target:impactor ratio of equilibrating silicate, and depth of equilibration
370 (Figure 6). These processes will all trade off with one another, and therefore can not be well-
371 constrained at this time. Two processes do not fall on this axis (the temperature of equilibration
372 and the oxidation state of accreting material) (Figure 6), so they will not exhibit these tradeoffs
373 and may be better constrained by the available data (Section 5.2).
374 For example, in the case of partial metal equilibration, the mantle composition can be
375 largely recovered by simultaneously shifting the equilibration to greater depth. Though the same
376 amount of incoming metal is added to the core without equilibrating with silicate, the portion that
377 does so equilibrates at higher pressure and temperature. Therefore, relative to results from the
378 reference set of parameters, the core in this case retains partly a lower *P*-*T* equilibration signature
379 (the portion that does not equilibrate) and partly a higher *P*-*T* equilibration signature (the portion
380 that does equilibrate), averaging out to approximately the same composition. All elements
381 modeled here exhibit this tradeoff, and/or show too little variability with these parameters to
382 provide constraints.
383 Figure 7 illustrates this tradeoff between depth and degree of equilibration, showing the
384 compositions (averaged over all Earth analogues) that result if the degree of metal equilibration
385 is varied with all other parameters held fixed to their reference values (closed symbols),
386 compared to the effects of simultaneously varying the depth of equilibration to hold the mantle
387 NiO content fixed (open symbols). Increasing the depth while decreasing the degree of
388 equilibration results in nearly the same core and mantle compositions as in the case of total

389 equilibration, down to ~30% of incoming metal equilibrating. This illustrates the robustness of
390 our conclusion that the core's density deficit can be accounted for nearly entirely by Si and O,
391 even with partial equilibration of the metal. A similar tradeoff exists with the mass of
392 equilibrating silicate (Figure 6): decreasing the fraction of metal that equilibrates can be
393 compensated for by increasing the mass of equilibrating silicate (Supplemental Text; Figure S7).
394
395 *5.2. Constraints on modeled parameters*
396 Constraints on modeled parameters are summarized in Table 1. Models in which the
397 Earth accretes mostly from oxidized materials are unsuccessful at reproducing geochemical and
398 geophysical observations (Table 2), in agreement with the findings of Rubie et al. (2015).
399 Accretion from only reduced materials or with a step in oxidation state at 1.5, 2, or 2.5 AU are
400 all currently plausible, given the compositional variability produced by accretion history (Figure
401 6) and uncertainties in the core's light element composition.
402 Equilibration temperatures are unlikely to fall below the liquidus of Andrault et al.
403 (2011), but temperatures up to ~300–500 K higher than this liquidus are permitted; higher
404 temperatures than this would put too much Si and O in the core to match its observed density.
405 The higher end of this range implies an absence of S, C, and other light elements in the core.
406 The extent of metal equilibration is not tightly constrained, due to the tradeoff with
407 equilibration depth. However, the fraction of incoming metal that equilibrates must be above
408 ~30% for equilibration with the impactor silicate only (or ~20% for equilibration with twice as
409 much silicate), consistent with independent geochemical arguments based on the Hf–W and U–
410 Pb systems (Nimmo et al., 2010; Rudge et al., 2010); otherwise the mantle NiO and CoO
411 constraints can not be satisfied simultaneously with the density constraints on Si and O in the

412 core (Figure 7). The effective depth of equilibration is also variable, due to trade-offs with other
413 processes. An upper bound is ~75% of the core–mantle boundary pressure in the case of a low
414 degree of metal equilibration (Figure 7), while a lower bound is ~42% in the case of whole
415 mantle equilibration, or ~37% for whole mantle equilibration and temperatures 500 K above the
416 liquidus of Andrault et al. (2011) (Table S3). Greater depths of equilibration would result in too
417 much Si and O in the core (Figure 7), while shallower values can not reproduce the mantle's
418 composition. This upper bound is consistent with geochemical arguments against a whole-mantle
419 magma ocean from noble gas constraints (e.g., Tucker and Mukhopadhyay, 2014). From this
420 modeling the mass or target:impactor ratio of equilibrating silicate can not be constrained.
421
422 *5.3. Relative sensitivity to different processes*
423 Within the allowable parameter space, composition is most sensitive to the depth of
424 equilibration (e.g., ±1.7 wt% Si in the core) (Table 1; Figure 5). It is moderately sensitive to the
425 temperature distribution, oxidation state, fraction of metal that equilibrates, and mass of
426 equilibrating silicate (e.g., ±0.7–0.9 wt% Si in the core). The resulting compositions, especially
427 the core composition, are relatively insensitive to the target:impactor ratio of the equilibrating
428 silicate (for a fixed mass), and to the mass of equilibrating silicate beyond three times the
429 impactor silicate mass (e.g., ±0.06 wt% Si in the core).
430 Sensitivities to depth and temperature are element-specific (Figures S4 and S6). For
431 example, Si partitioning is strongly temperature dependent with little or no pressure dependence
432 (Fischer et al., 2015), so its temperature variation is extremely similar to its depth variation
433 (Figure 5a and k). On the other hand, Ni partitioning is very pressure dependent, but its variation

434 with temperature changes with pressure and even changes sign, so it has a weak temperature
435 dependence when integrated over core formation (Figure 5l).
436 Variability due to accretion history is ±0.7 wt% Si and ±700 ppm NiO for 1 $M_\oplus$ planets
437 with core formation modeled using the reference set of parameters, considering the aggregate of
438 all 1 $M_\oplus$ Earth analogues (e.g., the vertical spread in Figure 4 near 1 $M_\oplus$); this effect is similar
439 in magnitude to the influence of other processes. The impact history of a planet and the
440 provenance of its building blocks determine the equilibration depth and the oxidation state of
441 accreted material, in turn affecting all aspects of planetary composition. Accretion is a highly
442 stochastic process, and the Earth is not necessarily the most likely outcome of its initial
443 conditions (Fischer and Ciesla, 2014). Therefore, it is important to consider a variety of possible
444 growth histories for the Earth as we have done here, to capture the range of possible outcomes.
445
446 *5.4. Assumptions, limitations, and simplifications of the modeling*
447 It is important to recognize the various limitations and simplifications inherent in this
448 modeling. For example, equilibration occurs at a fixed fraction of the target's core–mantle
449 boundary pressure. This is an approximation, since the depth of a magma ocean should depend in
450 a complex way on impactor size; time since the last impact; velocities, angles, and spatial
451 distribution of impacts; atmosphere; and other factors (e.g., Abe and Matsui, 1985; Solomatov,
452 2007). The amounts of metal and silicate that equilibrate are also likely variable (e.g., Deguen et
453 al., 2011, 2014). Modeling metal–silicate equilibration as occurring at a single pressure and
454 temperature for each impact, while an improvement over earlier models, is likely a
455 simplification. The *P*-*T* signature that a parcel of incoming metal retains should depend on the
456 degree of emulsification of the metal upon impact, as well as the time it takes to reach the base of

a magma ocean and then to descend to the core, and how these timescales compare to the mixing timescales of the magma ocean and the incoming metal (e.g., Deguen et al., 2011, 2014; Rubie et al., 2003). The largest impacts, such as the Moon-forming impact, may have exhibited qualitatively different partitioning behavior, such as increased depth of equilibration and reduced degree of equilibration (e.g., Tonks and Melosh, 1993). However, since there is a strong tradeoff between these two factors (Section 5.1), this model may be broadly capturing the chemical consequences accurately.

This modeling is based on only two oxidation states of starting materials, whereas meteorites show a wide range of variability (e.g., Righter and Neff, 2007). It is likely that Earth also accreted material with intermediate oxidation states, possibly a small amount of more oxidized material than considered here, and possibly material whose composition is significantly different from a CI chondrite. These cases will be explored in future work.

5.5. Future directions

In addition to revisiting the current simplifications and assumptions of this modeling (Section 5.4), more experimental partitioning data at the most extreme conditions of this modeling (~75–135 GPa) are needed; at present, there is only one published liquid metal–liquid silicate partitioning experiment from $P > 75$ GPa (Fischer et al., 2015). Data from $P > 25$ GPa are also needed on the valences of some trace elements (e.g., Walter and Cottrell, 2013) and the effects of S and C on the partitioning of other elements, which may help explain the modeled V and Cr contents of the mantle (e.g., Chabot and Agee, 2003; Mann et al., 2009; Wood et al., 2014), constrain the abundances of C and S in the core, and verify the uniqueness of the present solution that the core's density deficit can be mostly explained by Si and O. It is possible that the

480 presence of C and/or S will allow an alternative hypothesis, if these elements significantly
481 change the siderophility of Si and/or O.

482 Independent constraints are needed to resolve the strong tradeoff between depth of
483 equilibration and amounts of metal and silicate that equilibrate (Figures 6–7). Isotopic systems
484 such as Hf–W may be helpful in constraining the fraction of metal that equilibrates (e.g., Nimmo
485 et al., 2010), while fluid dynamics models and experiments can inform the masses of metal and
486 silicate that interact (e.g., Deguen et al., 2011, 2014), and impact modeling can constrain the
487 depth of melting that occurs (e.g., O'Keefe and Ahrens, 1994). These are some of the factors to
488 which the resulting composition is most sensitive (Table 1), so this is a particularly important
489 research direction.

490 This modeling can be readily applied to other types of accretion simulations, such as the
491 Grand Tack model (Walsh et al., 2011) or other Solar System configurations that may be
492 developed in the future. Effects of other factors like the initial mass distribution in the Solar
493 System, masses and number of bodies, embryos:planetesimals total mass ratio, growth
494 timescales, and delivery of more material from the outer Solar System could be explored using
495 different *N*-body simulations. Using a stricter definition of an "Earth analogue" may decrease the
496 variability due to accretion history as more *N*-body simulations become available. This modeling
497 can also be applied to other terrestrial planets to explore systematic variations in composition and
498 differentiation processes with planetary mass or semimajor axis, for example, though
499 comparisons to Mars and Mercury will require a larger number of simulations that form realistic
500 analogues with smaller initial bodies.

501 The modeled core mass fractions are slightly lower than that of the Earth's (~0.27–0.29
502 versus 0.32, Table S3). This suggests that either the Earth formed largely from more metal-rich

503 building blocks than those tested here, or that the Earth and/or its building blocks experienced
504 preferential loss of silicate during fragmenting collisions (e.g., Chambers, 2013), which were not
505 included in the *N*-body simulations on which this modeling is based. Future work should test
506 these hypotheses.
507 Finally, this modeling predicts substantial quantities of Si and O in the core. Mineral
508 physics results, such as measurements of phase diagrams, densities, and sound velocities of Si-
509 and O-rich alloys, can be used to verify these findings and constrain the abundances of minor
510 light elements in the core, such as S, C, and H.
511
512 **6. Conclusions**
513 The modeling presented here reproduces the Earth's measured mantle composition,
514 including important trace elements Ni and Co, and gives a plausible core light element
515 composition (in terms of density) with the same set of modeling parameters. This result lends
516 support to the methods used and implies that the core's light element budget is likely dominated
517 by silicon and oxygen. We have systematically explored the effects of a variety of processes on
518 the resulting core and mantle compositions, then used these results to test for tradeoffs between
519 processes, their plausible ranges, and the sensitivity of composition to different factors. There is
520 a strong tradeoff between the depth of equilibration and the amounts of metal and silicate that
521 equilibrate, while these factors do not trade off with the initial distribution of oxidation states of
522 materials, and only weakly trade off with equilibration temperature. These relationships allow us
523 to determine that the Earth accreted mostly from fairly reduced materials (~IW–3.5) and that
524 equilibration temperatures were likely near or slightly higher (<300–500 K) than the mantle
525 liquidus of Andrault et al. (2011). Processes with strong tradeoffs are excellent targets for future

studies, because they are the least constrained and their investigation will provide the greatest insight into the mechanism of core formation on Earth and other terrestrial planets. Core and mantle compositions are most sensitive to the depth of equilibration, amount of equilibrating material, and accretion history for plausible ranges of parameters, so future studies aiming to understand these processes will be the most successful at constraining the core's composition.

Acknowledgments

We thank two anonymous reviewers for their helpful comments and the editor for handling this manuscript. R.A.F. is grateful for support from a National Science Foundation (NSF) Graduate Research Fellowship, Illinois Space Grant Consortium Graduate Research Fellowship, International Centre for Diffraction Data Ludo Frevel Crystallography Scholarship, University of Chicago Plotnick Fellowship, American Association of University Women American Dissertation Fellowship, and an NSF postdoctoral fellowship (EAR-1452626). This work was also supported by NSF grant EAR-1427123 to A.J.C. and NASA grant NNX12AD59G to F.J.C.

References

Abe, Y., Matsui, T., 1985. The formation of an impact-generated H_2O atmosphere and its implications for the early thermal history of the Earth. J. Geophys. Res. 90, C545–C559, doi:10.1029/JB090iS02p0C545.

Abe, Y., Ohtani, E., Okuchi, T., Righter, K., Drake, M., 2000. Water in the early Earth. In: Canup, R.M., Righter, K. (Eds.), Origins of the Earth and Moon, University of Arizona Press, pp. 413–433.

548 Andrault, D., Bolfan-Casanova, N., Lo Nigro, G., Bouhifd, M.A., Garbarino, G., Mezouar, M.,
549 2011. Solidus and liquidus profiles of chondritic mantle: Implication for the melting of the
550 Earth across its history. Earth Planet. Sci. Lett. 304, 251–259,
551 doi:10.1016/j.epsl.2011.02.006.
552 Badro, J., Brodholt, J.P., Piet, H., Siebert, J., Ryerson, F.J., 2015. Core formation and core
553 composition from coupled geochemical and geophysical constraints. Proc. Natl. Acad. Sci.
554 USA 112, 12310–12314, doi:10.1073/pnas.1505672112.
555 Birch, F., 1952. Elasticity and constitution of the Earth's interior. J. Geophys. Res. 57, 227–286,
556 doi:10.1029/JZ057i002p00227.
557 Bond, J.C., Lauretta, D.S., O'Brien, D.P., 2010. Making the Earth: Combining dynamics and
558 chemistry in the Solar System. Icarus 205, 321–337, doi:10.1016/j.icarus.2009.07.037.
559 Bouhifd, M.A., Jephcoat, A.P., 2011. Convergence of Ni and Co metal–silicate partition
560 coefficients in the deep magma-ocean and coupled silicon–oxygen solubility in iron melts at
561 high pressures. Earth Planet. Sci. Lett. 307, 341–348, doi:10.1016/j.epsl.2011.05.006.
562 Burbine, T.H., O'Brien, K.M., 2004. Determining the possible building blocks of the Earth and
563 Mars. Meteorit. Planet. Sci. 39, 667–681, doi:10.1111/j.1945-5100.2004.tb00110.x.
564 Chabot, N.L., Agee, C.B., 2003. Core formation in the Earth and Moon: New experimental
565 constraints from V, Cr, and Mn. Geochim. Cosmochim. Acta 67, 2077–2091,
566 doi:10.1016/S0016-7037(02)01272-3.
567 Chambers, J.E., 2013. Late-stage planetary accretion including hit-and-run collisions and
568 fragmentation. Icarus 224, 43–56, doi:10.1016/j.icarus.2013.02.015.
569 Deguen, R., Olson, P., Cardin, P., 2011. Experiments on turbulent metal-silicate mixing in a
570 magma ocean. Earth Planet. Sci. Lett. 310, 303–313, doi:10.1016/j.epsl.2011.08.041.

571 Deguen, R., Landeau, M., Olson, P., 2014. Turbulent metal–silicate mixing, fragmentation, and
572 equilibration in magma oceans. Earth Planet. Sci. Lett. 391, 274–287,
573 doi:10.1016/j.epsl.2014.02.007.
574 Elser, S., Meyer, M.R., Moore, B., 2012. On the origin of elemental abundances in the terrestrial
575 planets. Icarus 221, 859–874, doi:10.1016/j.icarus.2012.09.016.
576 Fischer, R.A., Ciesla, F.J., 2014. Dynamics of the terrestrial planets from a large number of *N*-
577 body simulations. Earth Planet. Sci. Lett. 392, 28–38, doi:10.1016/j.epsl.2014.02.011.
578 Fischer, R.A., Campbell, A.J., Shofner, G.A., Lord, O.T., Dera, P., Prakapenka, V.B., 2011.
579 Equation of state and phase diagram of FeO. Earth Planet. Sci. Lett. 304, 496–502,
580 doi:10.1016/j.epsl.2011.02.025.
581 Fischer, R.A., Campbell, A.J., Reaman, D.M., Miller, N.A., Heinz, D.L., Dera, P., Prakapenka,
582 V.B., 2013. Phase relations in the Fe–FeSi system at high pressures and temperatures. Earth
583 Planet. Sci. Lett. 373, 54–64, doi:10.1016/j.epsl.2013.04.035.
584 Fischer, R.A., Campbell, A.J., Caracas, R., Reaman, D.M., Heinz, D.L., Dera, P., Prakapenka,
585 V.B., 2014. Equations of state in the Fe–FeSi system at high pressures and temperatures. J.
586 Geophys. Res. Solid Earth 119, 2810–2827, doi:10.1002/2013JB010898.
587 Fischer, R.A., Nakajima, Y., Campbell, A.J., Frost, D.J., Harries, D., Langenhorst, F., Miyajima,
588 N., Pollok, K., Rubie, D.C., 2015. High pressure metal–silicate partitioning of Ni, Co, V, Cr,
589 Si, and O. Geochim. Cosmochim. Acta 167, 177–194, doi:10.1016/j.gca.2015.06.026.
590 Fiquet, G., Auzende, A.L., Siebert, J., Corgne, A., Bureau, H., Ozawa, H., Garbarino, G., 2010.
591 Melting of peridotite to 140 gigapascals. Science 329, 1516–1518,
592 doi:10.1126/science.1192448.

593 Malavergne, V., Siebert, J., Guyot, F., Gautron, L., Combes, R., Hammouda, T., Borensztajn, S.,
594 Frost, D., Martinez, I., 2004. Si in the core? New high-pressure and high-temperature
595 experimental data. Geochim. Cosmochim. Acta 68, 4201–4211,
596 doi:10.1016/j.gca.2004.04.013.
597 Mann, U., Frost, D.J., Rubie, D.C., 2009. Evidence for high-pressure core–mantle differentiation
598 from the metal–silicate partitioning of lithophile and weakly-siderophile elements. Geochim.
599 Cosmochim. Acta 73, 7360–7386, doi:10.1016/j.gca.2009.08.006.
600 McDonough, W.F., 2003. Compositional model for the Earth's core. In: Carlson, R.W. (Ed.),
601 Treatise on Geochemistry, Vol. 2, Elsevier, pp. 547–568, doi:10.1016/B0-08-043751-
602 6/02015-6.
603 McDonough, W.F., Sun, S.-s., 1995. The composition of the Earth. Chem. Geol. 120, 223–253,
604 doi:10.1016/0009-2541(94)00140-4.
605 Nakajima, Y., Imada, S., Hirose, K., Komabayashi, T., Ozawa, H., Tateno, S., Tsutsui, S.,
606 Kuwayama, Y., Baron, A.Q.R., 2015. Carbon-depleted outer core revealed by sound velocity
607 measurements of liquid iron–carbon alloy. Nat. Commun. 6, 8942,
608 doi:10.1038/ncomms9942.
609 Nimmo, F., 2007. Energetics of the core. In: Olson, P. (Ed.), Treatise on Geophysics, Vol. 8,
610 Elsevier, pp. 31–65, doi:10.1016/B978-044452748-6.00128-0.
611 Nimmo, F., O'Brien, D.P., Kleine, T., 2010. Tungsten isotopic evolution during late-stage
612 accretion: Constraints on Earth–Moon equilibration. Earth Planet. Sci. Lett. 292, 363–370,
613 doi:10.1016/j.epsl.2010.02.003.
614 O'Keefe, J.D., Ahrens, T.J., 1994. Impact-induced melting of planetary surfaces. In: Dressler,
615 B.O., Grieve, R.A.F., Sharpton, V.L. (Eds.), Large Meterorite Impacts and Planetary

616 Evolution, Geological Society of America Special Paper 293, Boulder, CO, pp. 103–109,
617 doi:10.1130/SPE293-p103.
618 Poirier, J.-P., 1994. Light elements in the Earth's outer core: A critical review. Phys. Earth
619 Planet. Inter. 85, 319–337, doi:10.1016/0031-9201(94)90120-1.
620 Raymond, S.N., O'Brien, D.P., Morbidelli, A., Kaib, N.A., 2009. Building the terrestrial planets:
621 Constrained accretion in the inner Solar System. Icarus 203, 644–662,
622 doi:10.1016/j.icarus.2009.05.016.
623 Righter, K., 2015. Modeling siderophile elements during core formation and accretion, and the
624 role of the deep mantle and volatiles. Am. Mineral. 100, 1098–1109, doi:10.2138/am-2015-
625 5052.
626 Righter, K., Neff, K.E., 2007. Temperature and oxygen fugacity constraints on CK and R
627 chondrites and implications for water and oxidation in the early Solar System. Polar Sci. 1,
628 25–44, doi:10.1016/j.polar.2007.04.002.
629 Righter, K., Drake, M.J., Scott, E., 2006. Compositional relationships between meteorites and
630 terrestrial planets. In: Lauretta, D.S., McSween, H.Y. Jr. (Eds.), Meteorites and the Earth
631 Solar System II, University of Arizona Press, Tucson, pp. 803–828.
632 Ringwood, A.E., 1959. On the chemical evolution and densities of the planets. Geochim.
633 Cosmochim. Acta 15, 257–283, doi:10.1016/0016-7037(59)90062-6.
634 Rubie, D.C., Melosh, H.J., Reid, J.E., Liebske, C., Righter, K., 2003. Mechanisms of metal–
635 silicate equilibration in the terrestrial magma ocean. Earth Planet. Sci. Lett. 205, 239–255,
636 doi:10.1016/S0012-821X(02)01044-0.

637 Rubie, D.C., Frost, D.J., Mann, U., Asahara, Y., Nimmo, F., Tsuno, K., Kegler, Ph., Holzheid,
638 A., Palme, H., 2011. Heterogeneous accretion, composition and core–mantle differentiation
639 of the Earth. Earth Planet. Sci. Lett. 301, 31–42, doi:10.1016/j.epsl.2010.11.030.
640 Rubie, D.C., Jacobson, S.A., Morbidelli, A., O'Brien, D.P., Young, E.D., de Vries, J., Nimmo,
641 F., Palme, H., Frost, D.J., 2015. Accretion and differentiation of the terrestrial planets with
642 implications for the compositions of early-formed Solar System bodies and accretion of
643 water. Icarus 248, 89–108, doi:10.1016/j.icarus.2014.10.015.
644 Rudge, J.F., Kleine, T., Bourdon, B., 2010. Broad bounds on Earth's accretion and core
645 formation constrained by geochemical models. Nat. Geosci. 3, 439–443,
646 doi:10.1038/NGEO872.
647 Sata, N., Hirose, K., Shen, G., Nakajima, Y., Ohishi, Y., Hirao, N., 2010. Compression of FeSi,
648 Fe_3C, $Fe_{0.95}O$, and FeS under the core pressures and implication for light element in the
649 Earth's core. J. Geophys. Res. 115, B09204, doi:10.1029/2009JB006975.
650 Siebert, J., Badro, J., Antonangeli, D., Ryerson, F.J., 2012. Metal–silicate partitioning of Ni and
651 Co in a deep magma ocean. Earth Planet. Sci. Lett. 321–322, 189–197,
652 doi:10.1016/j.epsl.2012.01.013.
653 Siebert, J., Badro, J., Antonangeli, D., Ryerson, F.J., 2013. Terrestrial accretion under oxidizing
654 conditions. Science 339, 1194–1197, doi:10.1126/science.1227923.
655 Solomatov, V., 2007. Magma oceans and primordial mantle differentiation. In: Stevenson, D.J.
656 (Ed.), Treatise on Geophysics, Vol. 9, Elsevier, pp. 91–119, doi:10.1016/B978-044452748-
657 6.00141-3.
658 Tonks, W.B., Melosh, H.J., 1993. Magma ocean formation due to giant impacts. J. Geophys.
659 Res. 98, 5319–5333, doi:10.1029/92JE02726.

660 Tsiganis, K., Gomes, R., Morbidelli, A., Levison, H.F., 2005. Origin of the orbital architecture of
661 the giant planets of the Solar System. Nature 435, 459–461, doi:10.1038/nature03539.
662 Tucker, J.M., Mukhopadhyay, S., 2014. Evidence for multiple magma ocean outgassing and
663 atmospheric loss episodes from mantle noble gases. Earth Planet. Sci. Lett. 393, 254–265,
664 doi:10.1016/j.epsl.2014.02.050.
665 Wade, J., Wood, B.J., 2005. Core formation and the oxidation state of the Earth. Earth Planet.
666 Sci. Lett. 236, 78–95, doi:10.1016/j.epsl.2005.05.017.
667 Walsh, K.J., Morbidelli, A., Raymond, S.N., O'Brien, D.P., Mandell, A.M., 2011. A low mass
668 for Mars from Jupiter's early gas-driven migration. Nature 475, 206–209,
669 doi:10.1038/nature10201.
670 Walter, M.J., Cottrell, E., 2013. Assessing uncertainty in geochemical models for core formation
671 in Earth. Earth Planet. Sci. Lett. 365, 165–176, doi:10.1016/j.epsl.2013.01.014.
672 Wood, B.J., Li, J., Shahar, A., 2013. Carbon in the core: Its influence on the properties of core
673 and mantle. Rev. Mineral. Geochem. 75, 231–250, doi:10.2138/rmg.2013.75.8.
674 Wood, B.J., Kiseeva, E.S., Mirolo, F.J., 2014. Accretion and core formation: The effects of
675 sulfur on metal–silicate partition coefficients. Geochim. Cosmochim. Acta 145, 248–267,
676 doi:10.1016/j.gca.2014.09.002.
677 Zhang, Y., Sekine, T., He, H., Yu, Y., Liu, F., Zhang, M., 2014. Shock compression of Fe–Ni–Si
678 system to 280 GPa: Implications for the composition of the Earth's outer core. Geophys. Res.
679 Lett. 41, 4554–4559, doi:10.1002/2014GL060670.
680
681 **Figure captions**

682 **Figure 1:** Examples of information about the Earth's accretion history that can be obtained from
683 *N*-body simulations. Bottom panel: Mass evolution of the Earth analogue as a function of time
684 from three example simulations (dotted black, solid medium gray, and dashed light gray lines
685 correspond to different simulations). Top panel: Initial semimajor axis of each body accreted by
686 the Earth analogue in two of the same simulations (black and medium gray); the third simulation
687 is not shown for clarity. Large filled circles: Moon- to Mars-mass planetary embryos. Small open
688 circles: planetesimals (~0.001 $M_{\oplus}$).
689
690 **Figure 2:** Evolution of composition as the Earth grows. Results are shown for three of the
691 accretion simulations. Top panel: oxygen (navy blue) and silicon (red) in the core. Bottom panel:
692 NiO in the mantle (orange). Dotted, solid, and dashed lines correspond to the same example
693 simulations as shown in Figure 1. Each of these three *N*-body simulations produces an Earth
694 analogue with a mass of ~0.96 $M_{\oplus}$, whose core formation was modeled using the same reference
695 set of parameters (Table 1), so variability between them is due entirely to variations in accretion
696 history. Evolution of FeO content of the mantle for all 73 *N*-body simulations is shown in Figure
697 S1.
698
699 **Figure 3:** (a) The light element composition of Earth's core for different oxidation states of the
700 accreted material. Each histogram shows the final oxygen (navy blue) and silicon (red) contents
701 of the Earth's core, summarizing the aggregate results from all 73 *N*-body simulations of Fischer
702 and Ciesla (2014) that produce a realistic Earth analogue for a particular set of core formation
703 model conditions. Left panel: all accreted material is initially reduced (IW–3.5). Center panel:
704 reference parameters, in which material originating inside of 2 AU is reduced and material

705 originating outside of 2 AU is oxidized (IW–1.5). Right panel: all material is initially oxidized.
706 Other model parameters are held constant to their reference values. (b) Histograms of mantle
707 NiO (orange) and CoO (light blue) contents, showing results from the reference set of model
708 parameters. Shaded regions are Earth values from McDonough and Sun (1995). Values and
709 uncertainties are means and standard deviations of all 73 Earth analogues.
710
711 **Figure 4:** Final light element composition of the core as a function of Earth analogue mass for
712 different oxidation states of the accreted material. Each pair of Si and O data points in each panel
713 represents one of the 73 Earth analogues. Initial oxidation state of accreted material is the only
714 core formation model parameter varied between cases (panels); all other parameters were held
715 fixed at their reference values. Top panel: all reduced starting materials. Middle panel: reference
716 set of model parameters (step function in oxidation state of starting materials). Bottom panel: all
717 oxidized starting materials. Navy blue squares: silicon. Red diamonds: oxygen. Light element
718 content of the core is strongly, but not perfectly, correlated with planetary mass, showing that the
719 size of a planet largely controls its core Si and O contents but that accretion history also exerts an
720 influence.
721
722 **Figure 5:** Variations in NiO in the mantle (bottom row, orange circles) and Si in the core (top
723 row, red diamonds) with different processes. One parameter is varied at a time with all others
724 held constant at their reference values. Each data point represents an average of all 73 Earth
725 analogues and a given set of core formation model parameters, with error bars representing the
726 2σ variability due to accretion history for planets with masses of 0.9–1.1 $M_{\oplus}$. Labels on the plots
727 indicate endmember conditions. (a–b) Depth of equilibration, expressed as a fraction of the core–

mantle boundary pressure. (c–d) Initial oxygen fugacity distribution, ranging from all initially IW−1.5 to all initially IW−3.5. Intermediate values indicate the location of a step in initial oxygen fugacity from IW−3.5 to IW−1.5. (e–f) Fraction of incoming metal that equilibrates. (g–h) Target:impactor ratio of the equilibrating silicate, for a fixed equilibrating silicate mass of twice that of the impactor's silicate (in some impacts, this ratio was necessarily lower; Section 2). (i–j) Mass of equilibrating silicate, as a multiple of the impactor silicate mass. The impactor silicate always equilibrates; variable amounts of target silicate are added to vary the equilibrating silicate mass (in some impacts, this mass was necessarily lower; Section 2). (k–l) Temperatures of equilibration, with a ΔT of zero representing the mantle liquidus of Andrault et al. (2011). Orange shaded region is Earth value from McDonough and Sun (1995). Grey dashed lines indicate values from reference case. Greyed out regions indicate implausible parameter space (Table 1).

Figure 6: Covariance of mantle and core compositions caused by different accretion and differentiation processes, illustrating tradeoffs. Each data point represents an average of all 73 Earth analogues and a given set of core formation model parameters. All core formation model parameters were held fixed to their reference values except for the one parameter being varied along each line. Processes that vary from the lower left to the upper right reflect a shallower to deeper signature, respectively; processes that vary from the upper left to lower right reflect a reduced to oxidized signature, respectively. This figure illustrates the full range of parameter space explored (Table 1). Orange shaded region is Earth value from McDonough and Sun (1995). Grey dashed lines indicate values from reference set of model parameters. Black error

bars represent the 2σ variability due to accretion history for planets with masses of 0.9–1.1 $M_{\oplus}$ for the reference set of model parameters.

Figure 7: Variations in composition with partial equilibration of the metal at a fixed fractional depth (55% of the core–mantle boundary pressure, the reference value of this parameter), or with variable depth to maintain a constant NiO content of the mantle. All core formation model parameters were held fixed to their reference values except for the degree of metal equilibration (filled symbols and solid lines) or both the degree of metal equilibration and depth (open symbols and dashed lines, labels indicate the depth of equilibration expressed as a percentage of CMB pressure). Each data point represents the average of all 73 Earth analogues formed in the *N*-body simulations for a given set of core formation model parameters. Top panel: Si (red diamonds) and O (navy blue squares) in the core. Middle panel: CoO in the mantle (light blue triangles). Bottom panel: NiO in the mantle (orange circles). The tradeoff between depth and degree of equilibration is robust down to ~30% of incoming metal equilibrating, but lower degrees of equilibration result in too much light element in the core. All cases that produce the mantle's trace element composition result in enough Si and O in the core to approximately account for the core density deficit. Shaded regions are Earth values from McDonough and Sun (1995). Error bars represent the 2σ variability due to accretion history for planets with masses of 0.9–1.1 $M_{\oplus}$. Data points are slightly horizontally staggered for clarity.

Tables

772 **Table 1:** Reference values, ranges tested, and ranges allowed for all adjustable model
773 parameters, and sensitivity of mantle NiO and core Si contents to these processes over the
774 allowed ranges of each parameter. CMB, core–mantle boundary.
775

776

Parameter	Reference value	Range tested	Range allowed	Effect on mantle NiO	Effect on core Si
Depth of equilibration	55% of CMB pressure	20%–100% of CMB pressure	37–75% of CMB pressure	± 1200 ppm	± 1.7 wt%
Initial oxidation states	step function from IW–3.5 to IW–1.5 at 2 AU	all IW–3.5, all IW–1.5, or step at 1.5, 2, or 2.5 AU	all IW–3.5, or step at ≥ 1.5 AU	± 500 ppm	± 0.8 wt%
Fraction of incoming metal that equilibrates	1	0.15–1	0.2–1	± 600 ppm	± 0.9 wt%
Target:impactor ratio of equilibrating silicate (fixed mass)	0	0–16	0–infinite	± 140 ppm	± 0.06 wt%
Mass of equilibrating silicate	impactor's silicate mass	1–11× impactor silicate mass	up to whole mantle mass	± 900 ppm (± 90 ppm for >3× impactor silicate mass)	± 0.7 wt% (± 0.06 wt% for >3× impactor silicate mass)
Temperature of equilibration	liquidus of Andrault et al. (2011)	300 K below to 600 K above the liquidus of Andrault et al. (2011)	0–500 K above the liquidus of Andrault et al. (2011)	± 120 ppm	± 0.8 wt%
Accretion history	stochastic variations from *N*-body simulations			± 700 ppm	± 1.0 wt%

777

778 **Table 2:** Average core and mantle compositions produced in several models, compared to
779 observed values. All compositions are reported in weight percent. Earth's mantle composition is
780 from McDonough and Sun (1995). CMF, core mass fraction. fO_2 is bulk planetary oxidation state
781 calculated from Eq. 3. Values and uncertainties are averages and standard deviations of 73 *N*-
782 body simulations for a particular set of core formation model conditions. Reduced case: all
783 bodies initially at IW−3.5. Oxidized case: all bodies initially at IW−1.5. Reference model
784 parameters include a step function in initial oxidation state at 2 AU. All model parameters are
785 held fixed at their reference values except for the initial distribution of oxidation states.

	Reduced case	Reference model parameters	Oxidized case	Earth value
Mantle (wt%)				
SiO_2	47.4 ± 1.0	47.1 ± 0.9	42.65 ± 0.10	45.0
MgO	37.19 ± 0.17	36.2 ± 0.7	30.6 ± 0.6	37.9
FeO	6.5 ± 0.8	7.9 ± 1.1	18.9 ± 0.7	8.1
Al_2O_3	4.59 ± 0.02	4.47 ± 0.08	3.77 ± 0.07	4.45
CaO	3.721 ± 0.017	3.63 ± 0.07	3.06 ± 0.06	3.55
NiO	0.20 ± 0.10	0.25 ± 0.10	0.51 ± 0.11	0.25
CoO	0.010 ± 0.003	0.013 ± 0.004	0.030 ± 0.003	0.013
Nb_2O_5	$(9.1 \pm 0.2) \times 10^{-5}$	$(8.9 \pm 0.3) \times 10^{-5}$	$(8.23 \pm 0.16) \times 10^{-5}$	9.5×10^{-5}
Ta_2O_5	$(4.88 \pm 0.03) \times 10^{-6}$	$(4.76 \pm 0.09) \times 10^{-6}$	$(4.05 \pm 0.08) \times 10^{-6}$	4.53×10^{-6}
V_2O_3	0.0165 ± 0.0002	0.0162 ± 0.0003	0.0151 ± 0.0009	0.0121
CrO	0.415 ± 0.009	0.43 ± 0.02	0.51 ± 0.04	0.34
Core (wt%)				
Fe	86 ± 2	86 ± 2	86 ± 3	
Ni	5.2 ± 0.3	5.3 ± 0.3	6.5 ± 0.8	
Co	0.248 ± 0.008	0.252 ± 0.010	0.31 ± 0.03	
O	1.6 ± 1.0	1.9 ± 1.1	5 ± 2	
Si	6.3 ± 1.2	5.5 ± 1.4	2.1 ± 1.4	
Nb	$(1.4 \pm 0.3) \times 10^{-5}$	$(1.4 \pm 0.3) \times 10^{-5}$	$(1.0 \pm 0.2) \times 10^{-7}$	
Ta	$(8.4 \pm 1.6) \times 10^{-8}$	$(8.4 \pm 1.6) \times 10^{-8}$	$(2.2 \pm 0.2) \times 10^{-9}$	
V	0.0064 ± 0.0003	0.0065 ± 0.0004	0.005 ± 0.003	
Cr	0.679 ± 0.013	0.66 ± 0.02	0.46 ± 0.10	
CMF	0.307 ± 0.003	0.293 ± 0.010	0.194 ± 0.015	0.32
fO_2 (ΔIW)	–2.47 ± 0.16	–2.30 ± 0.15	–1.47 ± 0.05	

786

Figure 1

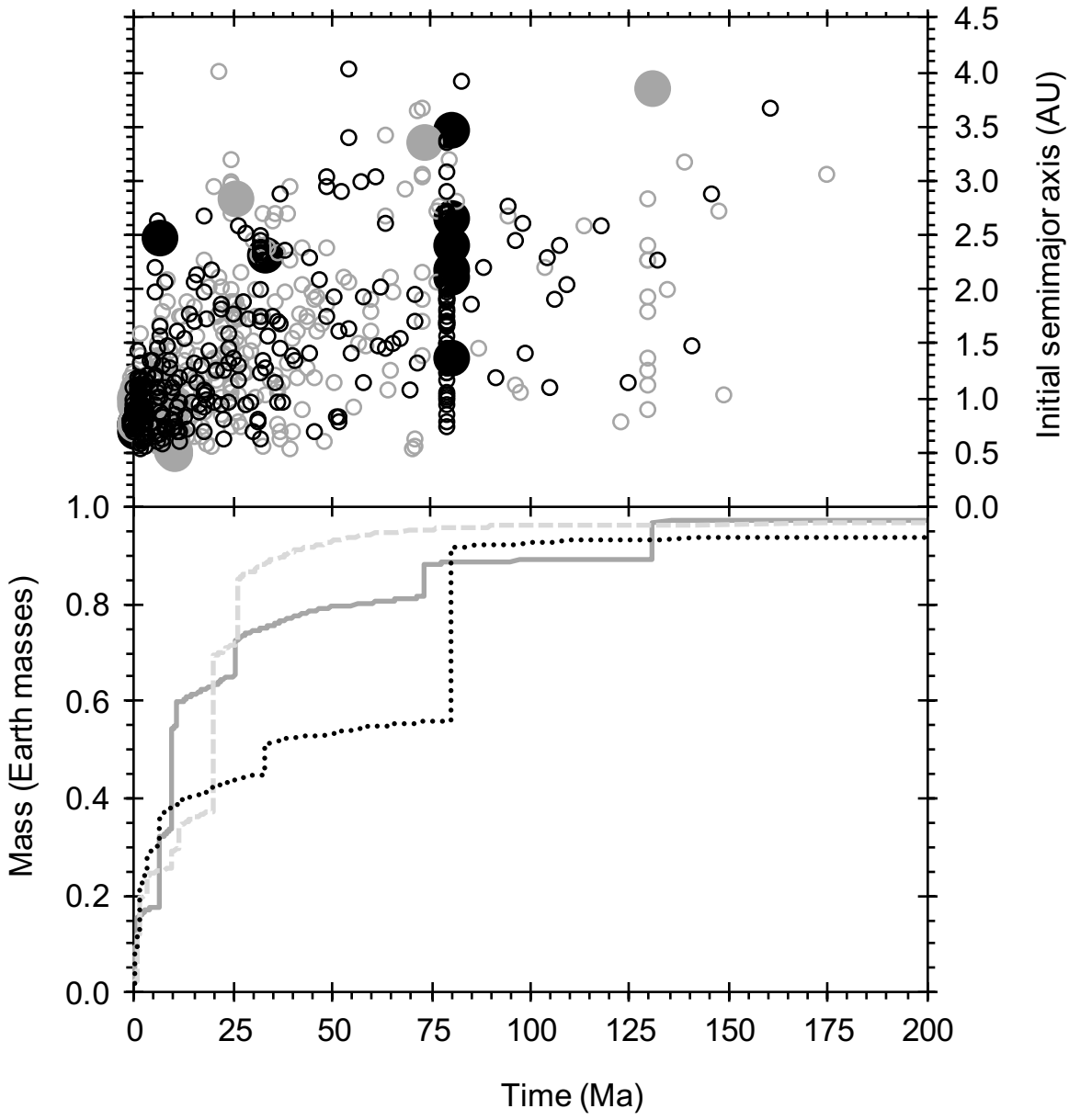
Initial semimajor axis (AU)
4.5
4.0
3.5
3.0
2.5
2.0
1.5
1.0
0.5
0.0
Mass (Earth masses)
1.0
0.8
0.6
0.4
0.2
0.0
0
25
50
75
100
125
150
175
200
Time (Ma)

Figure 2

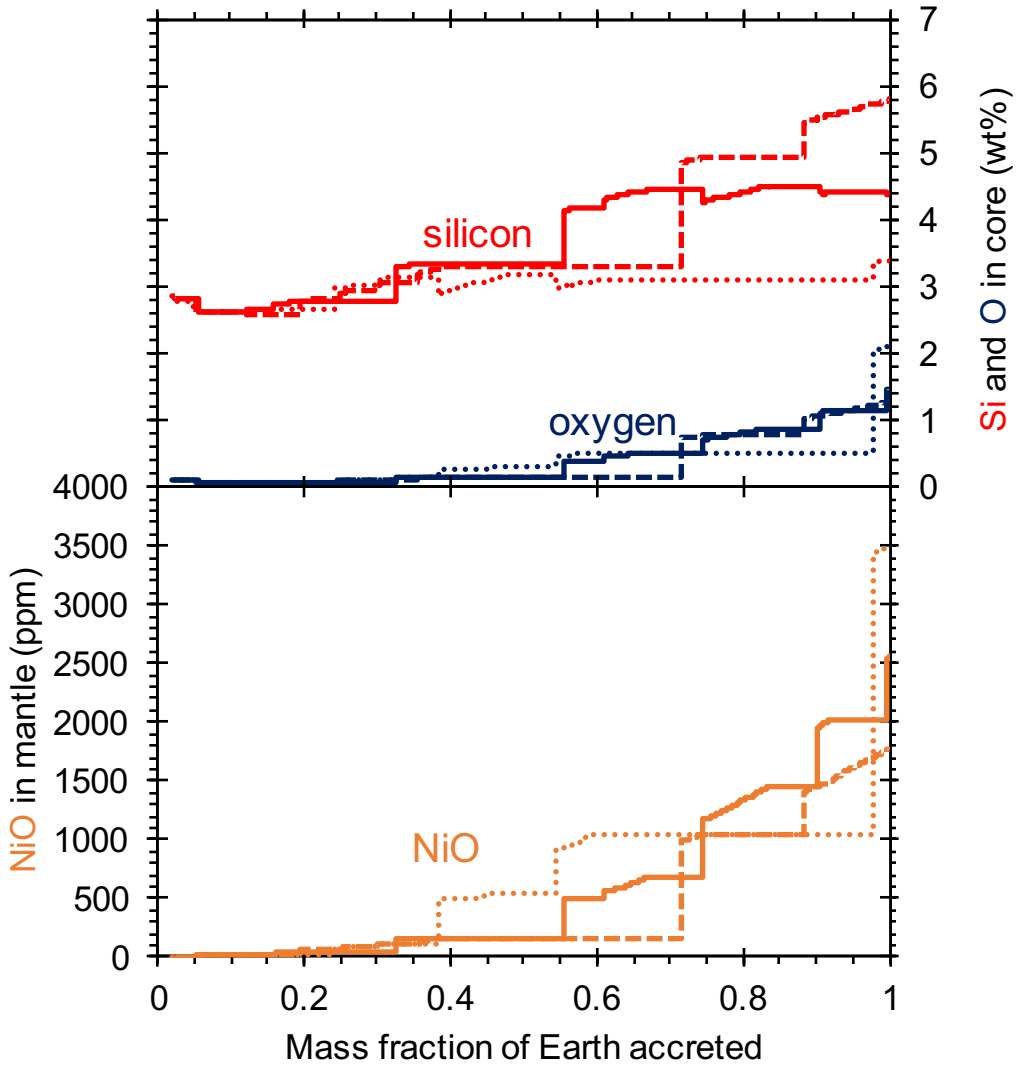
silicon
oxygen
NiO
Si and O in core (wt%)
NiO in mantle (ppm)
Mass fraction of Earth accreted
0
1
2
3
4
5
6
7
0
500
1000
1500
2000
2500
3000
3500
4000
0
0.2
0.4
0.6
0.8
1

Figure 3

(a)

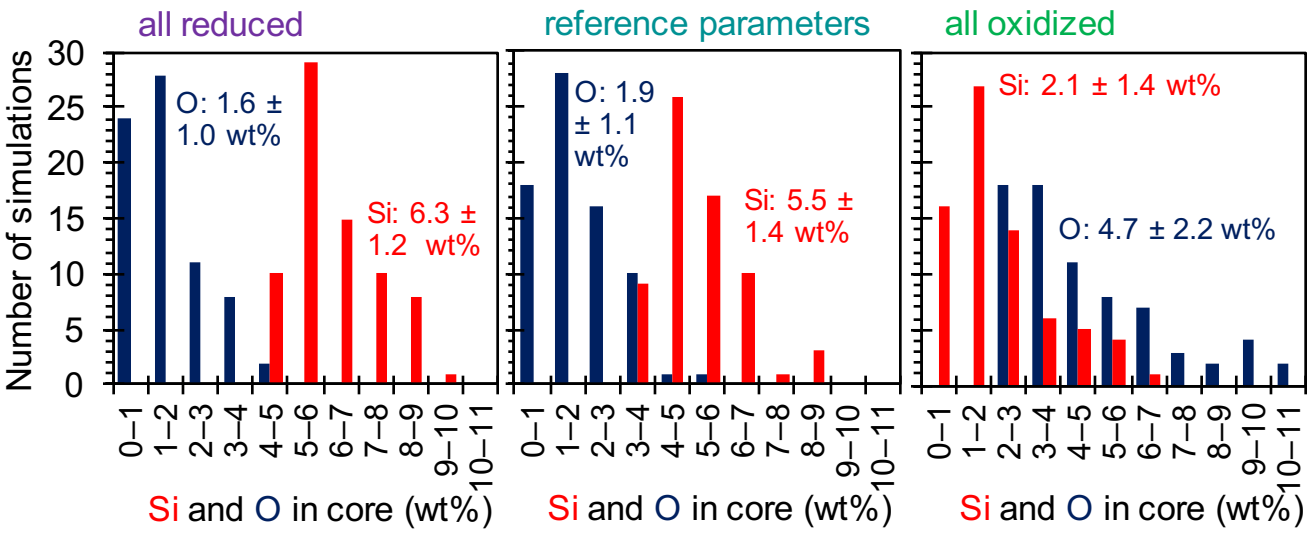
all reduced
reference parameters
all oxidized
Number of simulations
O: 1.6 ± 1.0 wt%
Si: 6.3 ± 1.2 wt%
O: 1.9 ± 1.1 wt%
Si: 5.5 ± 1.4 wt%
Si: 2.1 ± 1.4 wt%
O: 4.7 ± 2.2 wt%
Si and O in core (wt%)

(b)

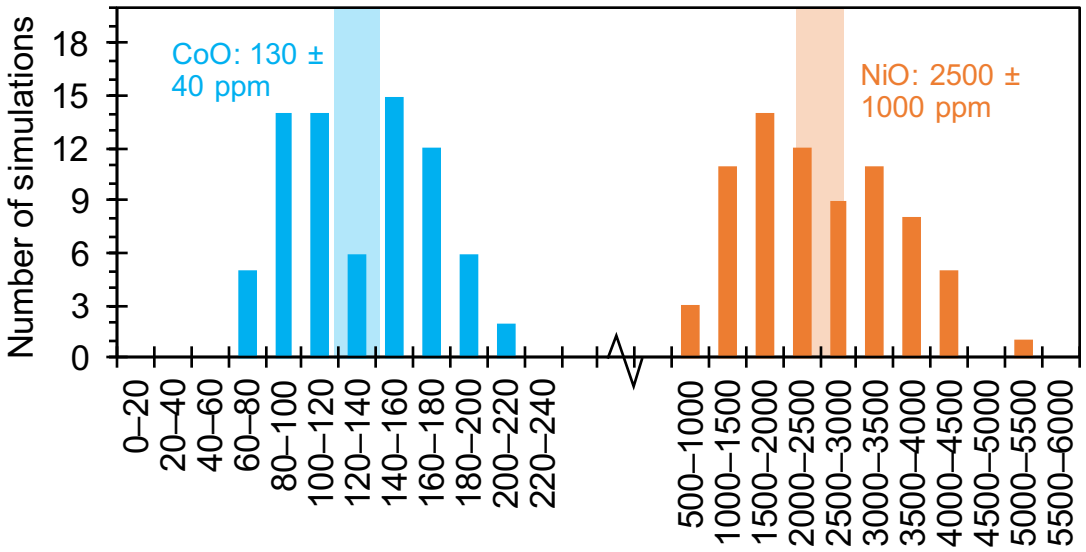
Number of simulations
CoO: 130 ± 40 ppm
NiO: 2500 ± 1000 ppm

Figure 4

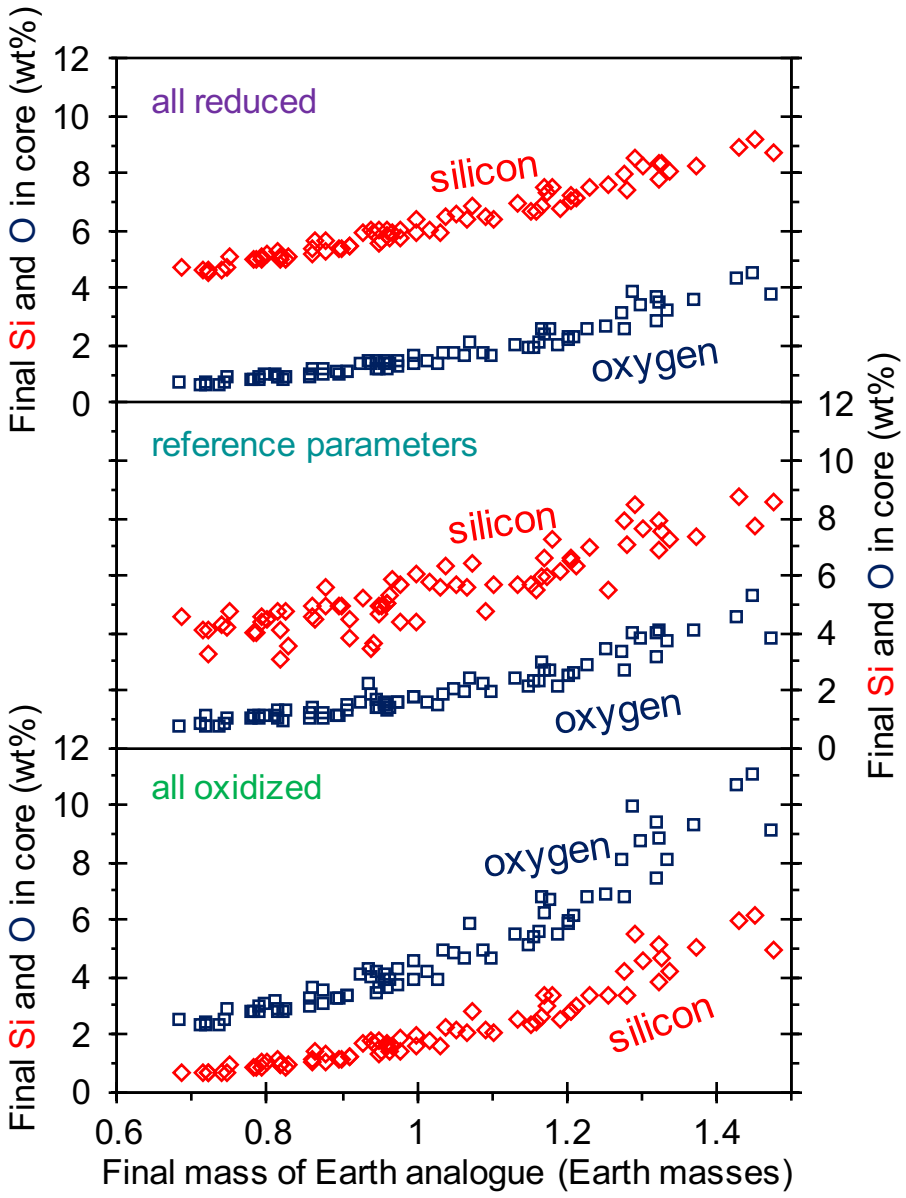
all reduced
silicon
oxygen
reference parameters
silicon
oxygen
all oxidized
oxygen
silicon
Final Si and O in core (wt%)
Final Si and O in core (wt%)
Final mass of Earth analogue (Earth masses)
0.6
0.8
1
1.2
1.4
0
2
4
6
8
10
12

Figure 5

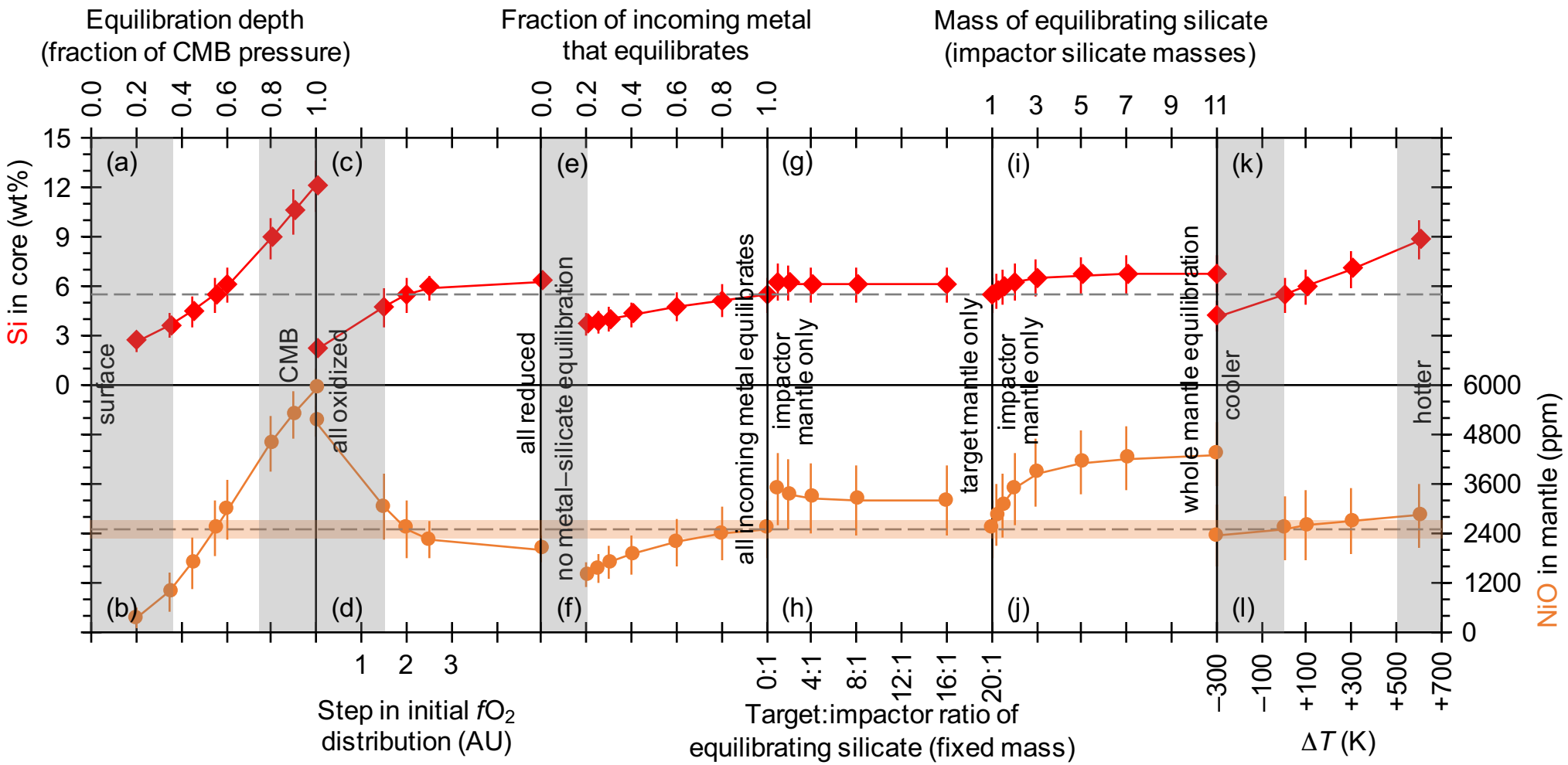
Equilibration depth
(fraction of CMB pressure)
Fraction of incoming metal
that equilibrates
Mass of equilibrating silicate
(impactor silicate masses)
Si in core (wt%)
NiO in mantle (ppm)
(a)
(b)
(c)
(d)
(e)
(f)
(g)
(h)
(i)
(j)
(k)
(l)
surface
CMB
all oxidized
all reduced
no metal–silicate equilibration
all incoming metal equilibrates
impactor mantle only
target mantle only
impactor mantle only
whole mantle equilibration
cooler
hotter
Step in initial fO_2 distribution (AU)
Target:impactor ratio of equilibrating silicate (fixed mass)
ΔT (K)

Figure 6

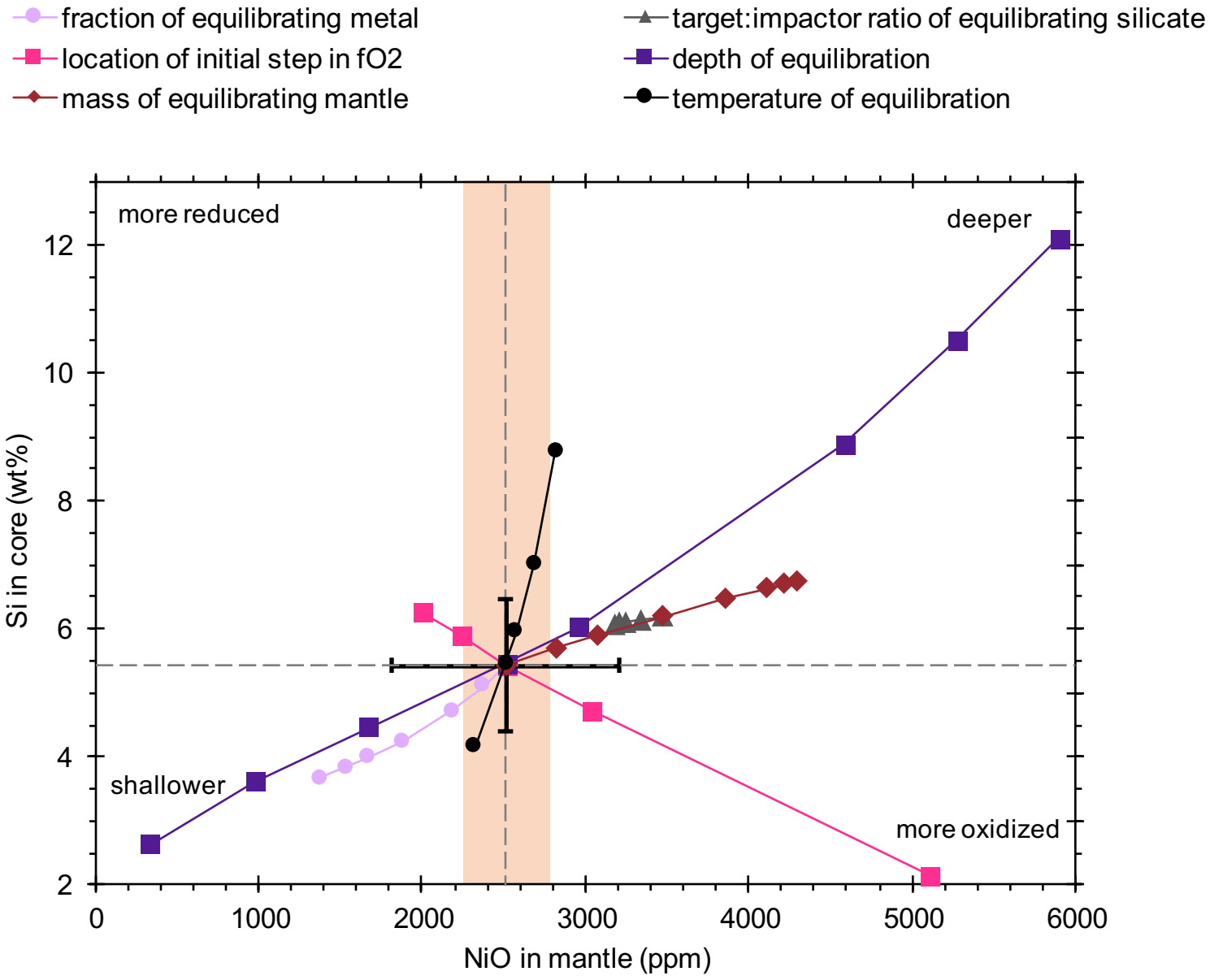
fraction of equilibrating metal
target:impactor ratio of equilibrating silicate
location of initial step in fO2
depth of equilibration
mass of equilibrating mantle
temperature of equilibration
more reduced
deeper
shallower
more oxidized
Si in core (wt%)
NiO in mantle (ppm)
2
4
6
8
10
12
0
1000
2000
3000
4000
5000
6000

Figure 7

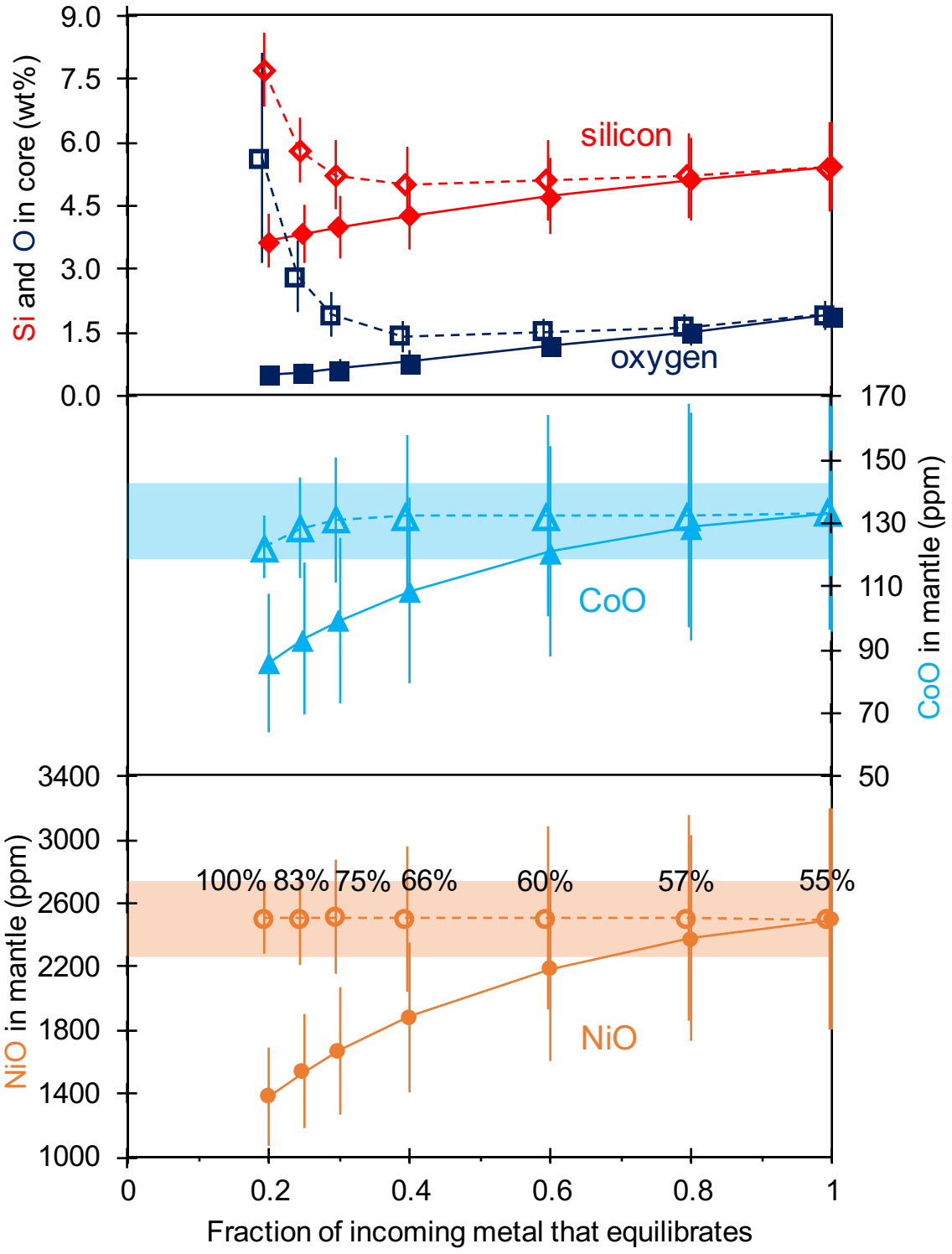
Si and O in core (wt%)
9.0
7.5
6.0
4.5
3.0
1.5
0.0
silicon
oxygen
CoO
CoO in mantle (ppm)
170
150
130
110
90
70
50
NiO in mantle (ppm)
3400
3000
2600
2200
1800
1400
1000
100%
83%
75%
66%
60%
57%
55%
NiO
0
0.2
0.4
0.6
0.8
1
Fraction of incoming metal that equilibrates